proceedings

Proceedings

Selecting the Optimal Use of the Geothermal Energy Produced with a Deep Borehole Heat Exchanger: Exergy Performance †

Claudio Alimonti [1], Paolo Conti [2] and Elena Soldo [1,*]

[1] Departement of Chemical Engineering Materials Environment, University of Rome—DICMA, Via Eudossiana 18, 00184 ROMA, Italy; claudio.alimonti@uniroma1.it

[2] Department of Energy,Systems,Territory and Construction Engineering (DESTEC), University of Pisa—DESTEC, Largo Lucio Lazzarino, 56122 Pisa, Italy; paolo.conti@unipi.it

* Correspondence: elena.soldo@uniroma1.it

† Presented at the First World Energies Forum, 14 September–5 October 2020; Available online: https://wef.sciforum.net/.for every paper.

Published: 11 September 2020

Abstract: Geothermal sector has a strength point respect to other renewable energy sources: the availability of a wide range of both thermal and power applications depending on source temperature. Several researches have been focused on the possibility to produce geothermal energy without brine extraction, by means of a deep borehole heat exchanger. This solution may be the key to increase the social acceptance, to reduce environmental impact of geothermal projects, and to exploit the unconventional geothermal systems, where the extraction of brines in technically complex. In this work, exergy efficiency has been used to investigate the best utilization strategy downstream the deep borehole heat exchanger. Five configurations have been analyzed: a district heating plant, an absorption cooling plant, an Organic Rankine Cycle, a cascade system composed by district heat and absorption chiller, a cascade system composed by the Organic Rankine plant and the district heating plant. District heating results a promising and robust solution: it ensures high energy capacities per well depth and high exergy efficiency. Power production shows performances in line with typical geothermal binary plants, but the system capacity per well depth is low and the complexity increases both irreversibilities and sensibility to operative and source conditions.

Keywords: geothermal energy; exergy; ORC; district heating; absorption cooling plant; deep borehole heat exchanger

1. Introduction

The geothermal energy is a sustainable, renewable and green energy source, but unfortunately underused. In 2018, the globally installed capacity of geothermal energy was 13.3 GW, only 0.57% of the total capacity of renewable energy sources [1]. This explains why the R&D areas of geothermal companies are focusing their efforts on finding new strategies to increase geothermal development. The main obstacles to the growth of the geothermal sector are the costs and risk related to exploration and drilling phases, and the absence of social consensus among population. An interesting solution proposed by several authors since 2000, i.e., [2–7], is the use of a zero-mass extraction device. The plant is a coaxial heat exchanger made of steel (Figure 1), which avoid all the risks (corrosion, scaling, subsidence, vapour emissions, micro-seismicity) and the costs related to the extraction and reinjection of brines. A heat carrier fluid is pumped in the external annulus that is separated by an insulator from the internal pipe, in which the fluid flows up to the bottomhole.

The scientific works have been demonstrated the feasibility of geothermal energy production via the deep borehole heat exchanger (DBHE) (or WellBore Heat eXchanger (WBHX) as is named by [8] and 5 pilot tests have been realized [9–14] consider the DBHE very promising for volcanic geothermal systems where the extraction of brines entails several issues. The use of the DBHE to repurpose depleted oil&gas wells has been also proposed by [15–20]. In fact, in hydrocarbons fields, a great amount of hot water is often present and the exploration, drilling and construction steps have been concluded.

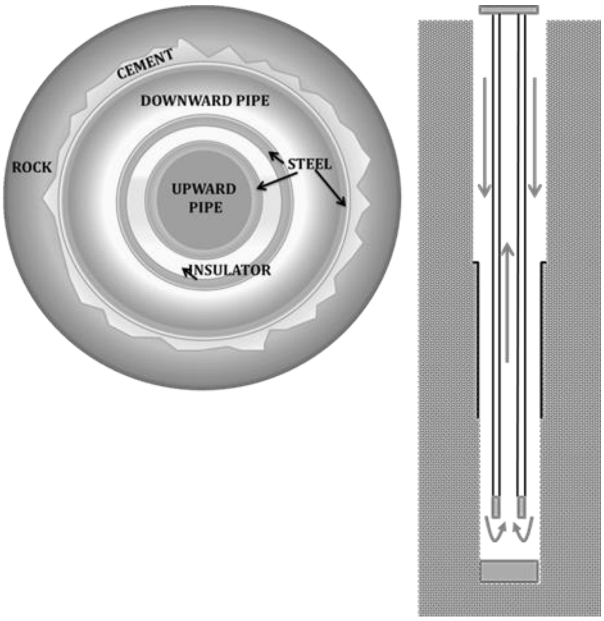

Figure 1. The deep borehole heat exchanger.

The main limit of the DBHE plant is the pure conductive heat extraction, which limits very much the heat effectiveness respect to the conventional plants. Therefore, regarding the final use of the extracted heat, [3,5,8,15,19,20] have evaluated the potential electricity production via ORC plants with maximum values of 350 kW. In other studies the heating and cooling applications are recommended for the final use, see [9,10,21,17,22].

The sector of buildings air-conditioning is particularly promising for geothermal resources, which can be used to satisfy the thermal request (heat, cool, and hot water) of buildings with no GHG emissions and independently by weather conditions, thus fostering the energy independence of countries.

The target of this work is to identify the optimal final use for the geothermal energy produced by a deep borehole heat exchanger. Five utilization layouts have been considered in the analysis: a district heating (DH) plant, an absorption-chiller (ABSC) plant, a cascade system composed by a DH plant and an ABSC plant, an Organic Rankine Cycle (ORC) plant, a cascade system composed by an ORC plant and a DH plant. A sensitivity analysis has been also carried out, changing the ground properties, the heat exchanger parameters, the operating temperatures of the DH and the ABSC plants.

The authors consider the exergy analysis the most suitable method to evaluate a system by a thermodynamic point of view. The exergy also includes a part that cannot be transformed in work, whereas the exergy is the available work. It is a measure of the maximum work output that could theoretically be obtained from a system interacting with a given environment (which is at constant pressure p_a and temperature T_a) [23,24]. The exergy balance takes also into account the irreversible production of entropy, thus identifying both maximum theoretical performance and the inefficiencies of a system.

The geothermal literature involving the exergy is very large. It includes the classification of resources with exergy [25–27] the exergy analysis of geothermal power plants [23,28–30], and the low enthalpy applications (ground source heat pumps, district heating and cooling, thermal storage), see [31–35]. The literature regarding the deep borehole heat exchanger reports only a few works [6,18,36] that include a thermodynamic assessment based on exergy balance: all of them analyze a DBHE connected to an Organic Rankin Cycle plant.

The present paper proposes a new approach for the sector of deep borehole heat exchangers and the final target is to identify the best implementation technology for a DBHE with specified conditions.

2. Materials and Methods

A homogenous performance index must be considered to properly compare different utilization strategies for WBHX technology. In this work, we refer to exergy concept that is widely applied in the energy sector to compare different energy forms (e.g., power and heat), systems and applications (e.g., power production, building cooling services, district heating networks). The exergy also referred to as “availability”, is a measure of the maximum work output that could theoretically be obtained from any thermodynamic system interacting with a reference environment (i.e., the dead state). Similarly, the exergy represents the minimum work that must be provided to any thermodynamic system to bring it from the dead state to a final energy state. Exergy analysis is an established methodology to investigate the quality of energy conversion processes as it can find irreversibilities and exergy losses occurring at each step and/or component [37]. In this work, the exergy efficiency has been applied to measure the exploitation quality of a given availability of energy (i.e., geothermal source) according to the utilization scenario.

We compare the exergy performance of five reference utilization plants to be coupled with WBHX technology. The reference systems are representative of possible employment strategies for geothermal energy, namely: power production, thermal uses, cascade and/or hybrid applications. Figure 2 show the reference layouts and the main related variables: (a) district heating; (b) absorption cooling plant; (c) an ORC power plant; (d) a cascade system composed by a cooling plant and a DH system (e) a cascade system composed by an ORC power plant coupled with a DH system at the outlet section of the turbine.

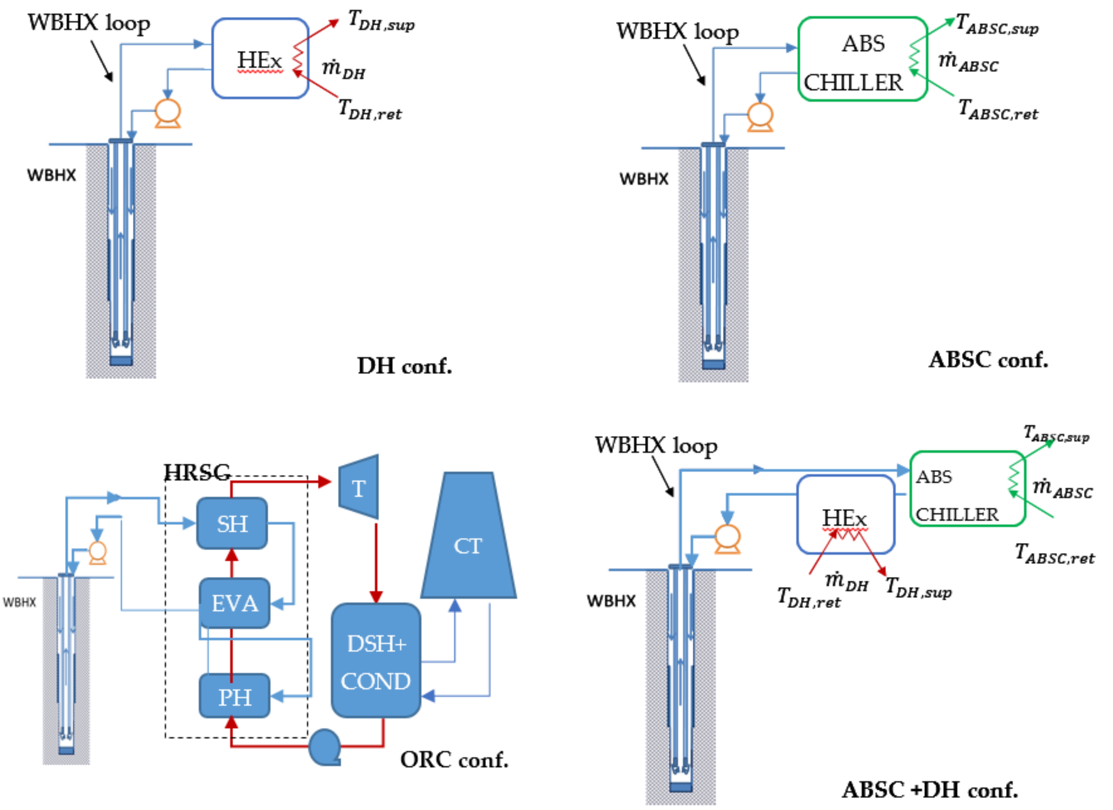

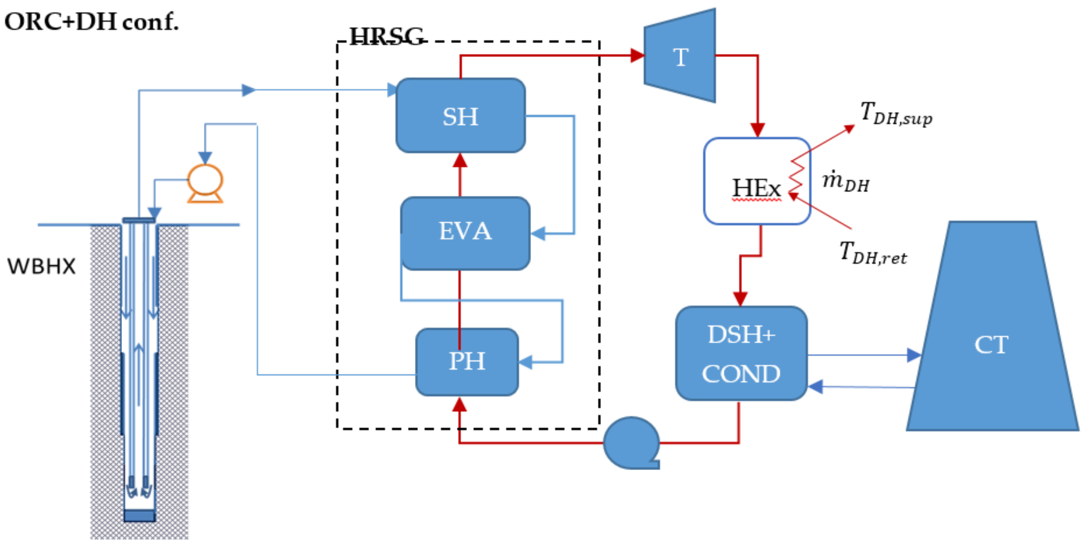

Figure 2. Reference utilization strategies and systems layout.

All the components of the systems in Figure 2 are evaluated at the nominal working conditions, through zero-dimensional steady-state mass, energy, and exergy balances, together with the overall rate equation for the heat exchangers. Thermo-physical properties of water and ORC working fluid are evaluated as a function of temperature and pressure, through the widespread software REFPROP [38]. The details on assumptions and components models are provided in [36]. Here, we recall the main modelling strategy of each component:

- Undisturbed/far-field ground temperature: the ground source is precautionary assumed as a purely conductive media. The far-field ground temperature profile is assumed as a linear function of the depth with a surface value of 25 °C (reference ambient temperature) and a constant temperature gradient over the z-direction, Kg. The values of K_g, and α_g are objective of the next sensitivity analysis.
- WBHX: the thermal power exchanged between the circulating fluid and the far-field ground temperature is evaluated through a series of equivalent thermal resistances. Axial effects are neglected, however, the temperature evolution of the fluid along the WHBX ducts are evaluated through the so-called "quasi-3D approach" [36,39]. At a given depth, *z*, the following differential equation applies:

$$\begin{cases} \dot{m}_w c_w \dfrac{dT_{w,dw}}{dz}(z) = \dfrac{T_s(z) - T_{w,dw}(z)}{R_a} - \dfrac{T_{w,dw}(z) - T_{w,uw}(z)}{R_b} \\ -\dot{m}_w c_w \dfrac{dT_{w,uw}}{dz}(z) = \dfrac{T_{w,dw}(z) - T_{w,uw}(z)}{R_b} \end{cases} \tag{1}$$

where R_a and R_b correspond to the resistances shown in Figure 3. R_s is the transient thermal resistance of the ground: it depends on ground thermophysical properties and the WBHX operation time [15,40]. In this work, we refer to a year of operation as it corresponds to the period required to get sufficiently close to the steady-state value. Further details are provided in [15,36]. The integration of the set of Equation (1) between the inlet and outlet sections of the WBHX provides the profile of the fluid temperature over the downward and upward ducts. The profile of the linear thermal power is evaluated accordingly. Friction losses and pumping requirements are evaluated through the classical Darcy–Weisbach equation using the Moody diagram for fully developed turbulent flows. Thermophysical properties of the water are assumed as dependent from temperature and pressure, therefore "thermosiphon effect" due to density variation is included in the model, affecting the energy required for pumping. Table 1 summarizes the diameters and the thermal properties of the WBHX layers (see Figure 3).

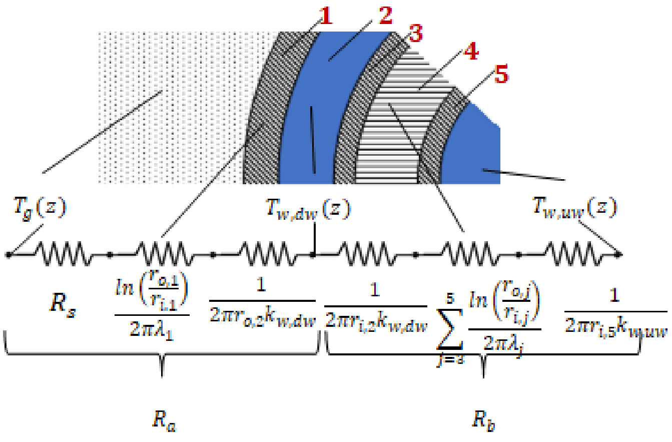

Figure 3. WBHX thermal resistance model.

Table 1. WBHX geometry and thermal properties.

Parameter	Value
D_o/D_i Layer 1	244.40/226.60 mm
D_o/D_i Layer 2	226.60/177.8 mm
D_o/D_i Layer 3	177.8/150.36 mm
D_o/D_i Layer 4	150.36/88.90 mm
D_o/D_i Layer 5	88.90/77.92 mm
Thermal conductivity steel (λ_1, λ_3, λ_5)	50 W/(mK)
Thermal conductivity insulation (λ_4)	0.04 W/(mK)

- District heating: the district heating network is modelled as water flow to be heated from 60 °C to 90 °C. The useful flow rate, m_{DH}, and the corresponding thermal power are calculated considering a heat transfer effectiveness of the main DH heat exchanger equal to 0.8. DH application is only considered if the production temperature of the WBHX must be higher than 100 °C.
- Absorption chiller: the end-user chiller loop works with a supply and return temperatures of 7 °C and 12 °C, respectively. The chiller is assumed as an indirect-fired unit, namely the generator is equipped with a heat exchanger that allows the energy transfer between the hot water from the WBHX loop and the refrigerant mixture (e.g., LiBr-H2O). The temperature required at the generator, T_{gen}, is assumed equal to 100 °C. The heat exchanger within the ABSC generator is assumed to be sufficiently long to ensure a unitary heat transfer effectiveness: in other words, the WBHX fluid leaves the absorption unit with a temperature equal to the one required in the ABSC generator. The performance of the chiller is evaluated through the Second-Law thermal efficiency method, according to sources temperatures and exergy efficiency, η^{II}_{ABSC}, assumed as constant and equal to 0.3.

$$EER = \eta^{II}_{ABSC}\left[\frac{\frac{1}{T_a}-\frac{1}{T_{gen}}}{\frac{1}{T_{ABSC,sup}}-\frac{1}{T_a}}\right] \quad (2)$$

- <u>ORC power plant and cooling tower:</u> following the results presented in [X], the considered working fluid is 2-methylpropane (isobutane). Depending on the temperature at the WBHX outlet section, the power of the Hirn cycle is calculated using the following assumption: a condenser temperature equal to 41 °C; a pinch point of the HRSG equal to 5 K; an approach point for all the heat exchangers equal to 10 K; an isentropic and electrical-mechanical efficiency of the turbine equal to 0.85 and 0.95, respectively; and an electrical-mechanical efficiency of the feeding pump equal to 0.6. The power required by the fans in the cooling tower is evaluated according to the model presented in the Appendix of [36]. For each tested configuration, the geometry of the finned surface (i.e., number of rows and number of ducts per row) and the frontal air velocity are optimized to minimize the electricity input, ensuring the required heat exchange at the condenser.

  The considered expressions of the exergy efficiency for each configuration is the following:

$$\eta_{DH}^{II} = \frac{\dot{m}_{DH}\left(ex_{DH,sup} - ex_{DH,ret}\right)}{Ex_{WBHX}^{\dot{Q}} + \dot{W}_{P,WBHX}} \tag{3}$$

$$\eta_{ABSC}^{II} = \frac{\dot{m}_{ABSC}\left(ex_{ABSC,sup} - ex_{ABSC,ret}\right)}{Ex_{WBHX}^{\dot{Q}} + \dot{W}_{P,WBHX}} \tag{4}$$

$$\eta_{ORC}^{II} = \frac{\dot{W}_{ORC,net} - \dot{W}_{P,WBHX}}{Ex_{WBHX}^{\dot{Q}}} \tag{5}$$

$$\eta_{ABSC+DH}^{II} = \frac{\dot{m}_{DH}\left(ex_{DH,sup} - ex_{DH,ret}\right) + \dot{m}_{ABSC}\left(ex_{ABSC,sup} - ex_{ABSC,ret}\right)}{Ex_{WBHX}^{\dot{Q}} + \dot{W}_{P,WBHX}} \tag{6}$$

$$\eta_{ORC+DH}^{II} = \frac{\dot{m}_{DH}\left(ex_{DH,sup} - ex_{DH,ret}\right) + \dot{W}_{ORC,net}}{Ex_{WBHX}^{\dot{Q}} + \dot{W}_{P,WBHX}} \tag{7}$$

where e_x is the physical exergy associated with the fluid stream m and $Ex_{WBHX}^{\dot{Q}}$ is the exergy associated to the heat flow between the undisturbed ground and the WBHX circulating fluid. W: is input or output electrical power or exergy. The reference environmental state is $T_a = 25$ °C and $p_a = 1$ bar.

This work presents a sensitivity analysis of the exergy efficiency indexes (see Equations (3)–(7)) depending on the characteristics of the ground source and WBHX geometry. The following parameters and ranges have been considered:

- Thermal diffusivity of the ground: $\alpha_g = \{10^{-7}; 5 \cdot 10^{-7}; 10^{-6}\}$ m²/s
- Thermal conductivity of the ground source: $\lambda_g = \{1; 2; 3\}$ W/(m K)
- Ground temperature gradient: $K_g = \{30; 60; 90; 120; 150\}$ K/km
- WBHX depth: H = {1, 2, 3, 4, 5} km

Globally, we tested 225 different configurations for each layout in Figure 2. For each tested configuration, the energy and the exergy balance of each component are evaluated through an in-house MATLAB® code.

Obviously, not all the 225 configurations are suitable for all the application strategies. To be included in the results, the following constraints must be met:

- The WBHX fluid must be at the liquid state. Proper work pressure and flow rate are thus evaluated for each configuration
- The ground temperature at the well bottom must be higher than 100 °C
- Configurations resulting in negative exergy efficiency are discarded (e.g., the auxiliary energy consumption exceeds power production).

3. Results

The boxplot in Figure 4 summarizes the distribution of the exergy efficiency obtained through the sensitivity analysis discussed in Section 2. The "boxplot" or "box-and-whisker" chart shows the distribution of the plotted quantity: the box goes from the 25th percentile, P_{25}, to the 75th percentile, P_{75}, of the distribution. The difference P_{75}-P_{25} is called the interquartile range (IQR) and represents a measure of the statistical dispersion. The middle line inside the box corresponds to the median value and the "X" marker corresponds to the mean value. The upper and lower limits of the whisker indicate the maximum and the minimum value, outlier excluded. The analysis of such a plot allows a better understanding of the general performances of the utilization strategies as it aggregates the results of many simulations, instead of a single case. However, we have selected one configuration to better discuss the main characteristics of WBHX employment according to the final user system (see Table 2).

We note that DH applications have a higher average value of η^{II} equal to 0.35 and an IQR_{DH} equal to 0.09. The latter value indicates a constant performance of the DH solution at various WBHX depth and geothermal source conditions. Additionally, DH shows the higher thermal power exchanged per well depth, as the lower inlet temperature (70 °C approx.) endorses the WBHX heat exchange. Table 2 also shows as the user equipment (the main HEx) has a limited irreversibility production concerning the well (45 kW vs. 18 kW).

The ABSC solution has low η^{II} values (μ_{ABSC} = 0.1) and a low dispersion (IQR_{ABSC} = 0.02). The exegetic performances are mainly affected by the user system technology, namely the absorption chiller. As shown in Table 2, the irreversibility generation in the WBHX is similar to the one occurring in the DH solution, but I_{user} almost doubles. Even in favourable operative conditions (T_a = 25 °C), ABSC does not seem a proper solution to be used alone because of the exergy efficiency of the absorption equipment (η^{II}_{ABSC} = 0.3).

Power production through ORC cycle has a IQR_{ORC} value equal to 0.07 and an average equal to μ_{ORC} =0.25. These results are coherent with the typical value of binary cycles for geothermal applications. Though electricity has high exergy value, energy production is low than thermal applications due to the energy efficiency of the ORC plant (~10 %). The heat transfer in the WBHX occurs with an irreversibility production similar to the DH and ABSC solution, but I_{user} has the maximum value among all the other utilization strategies.

The combined solution ABSC+DH has a wide range of η^{II} value, with average equal to $\mu_{ABSC+DH}$ = 0.24 and $IQR_{ABSC+DH}$ = 0.1. The high variability of performance is due to the relevance of "low-value" thermal exergy produced by the ABSC for the "high-value" thermal exergy produced by the DH heat exchanger located downstream the ABSC chiller. This ratio depends on WBHX flow rate as high m_w values increase DH thermal output and reduce the WBHX outlet temperature. The amount of cold energy production depends on a tradeoff between higher flow rate at the ABSC generator and lower useful temperature drop till $T_{ABSC,gen}$.

In the ORC+DH solution, exergy performances improve concerning the ORC solution thanks to the employment of a recovery heat exchange downstream power turbine. The average η_{II} value is equal to μ_{ORC+DH} = 0.34 and the IQR_{ORC+DH} is equal to 0.11. The performance increase is due to the lower heat to be discharged to the environment and associated lower exergy destruction and fewer fans power input. Table 2 confirms that power efficiency is practically the same as well as I_{WBHX} in both ORC and ORC+DH case, but I_{user}.

Table 2. Details on the performance of the five utilization strategies in the case H = 3 km, K_g = 60 K/km, λ_g = 2 W/(mK) and α_g = 10^{-7} m²/s.

	DH	ABSC	ORC	DH + ABSC	ORC + DH
η^{II}	0.43	0.10	0.21	0.33	0.24
$\dot{Q}_{DH,user}$	329 kW	-	-	207	8 kW
$\dot{Q}_{ABSC,user}$	-	184 kW	-	140 kW	-
$\dot{W}_{out,net}$	-	-	22 kW	-	22 kW
$\dot{Ex}_{out}$	47 kW	10 kW	22 kW	37 kW	24 kW

$\dot{E}x_{out}/\ \dot{Q}_{out}$ or $\dot{E}x_{out}/\dot{W}_{out,net}$	0.14	0.05	1	0.106	0.8
$\dot{m}_{WBHX}$	5.4 m³/h	5.4 m³/h	5.4 m³/h	5.4 m³/h	5.4 m³/h
$\dot{Q}_{WBHX}$	329 kW	196 kW	298 kW	356	247 kW
$T_{f,WBHX,in}$	73 °C	100 °C	80 °C	68 °C	90 °C
$T_{f,WBHX,out}$	125 °C	130 °C	126 °C	123 °C	130 °C
$Ex^{\dot{Q}}_{WBHX}$	109 kW	92 kW	105 kW	113 kW	99 kW
$\dot{I}_{WBHX}$	45 kW	48 kW	44 kW	45 kW	45 kW
$\dot{I}_{user}$	18 kW	35 kW	39 kW	31 kW	29 kW

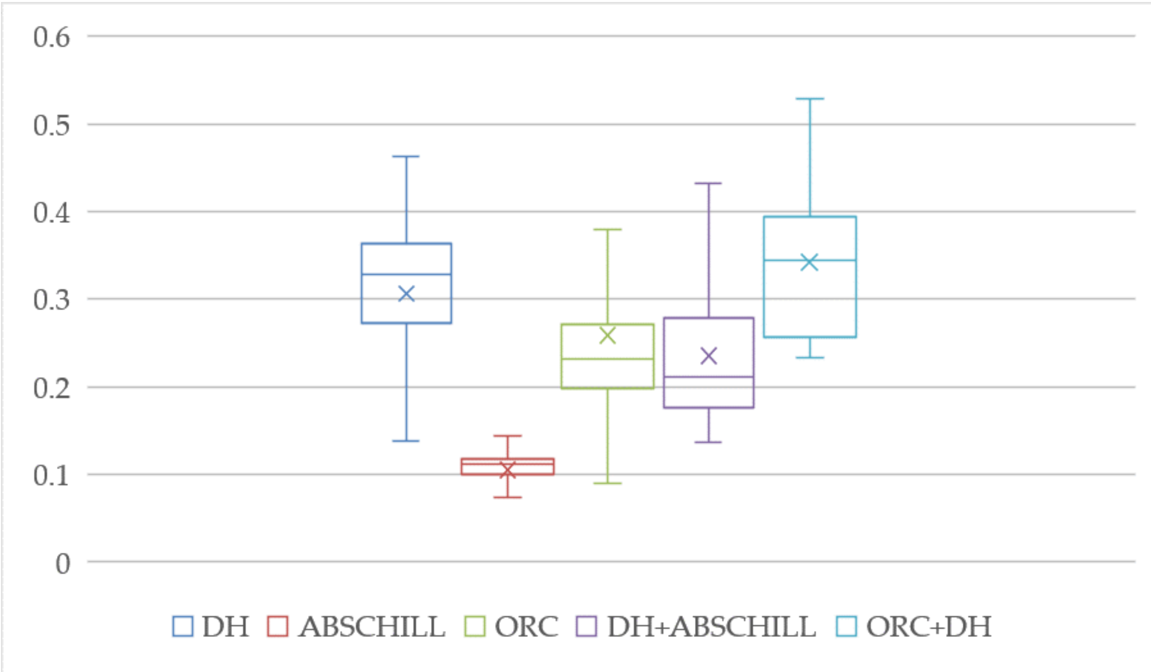

Figure 4. Boxplot of exergy efficiency in the 225 tested cases depending on final utilization strategy.

4. Discussion and Conclusions

This work has compared and discussed five possible utilization strategies of WBHX technology. Exergy efficiency has been chosen as the main performance index as it allows the comparison of heating, cooling and power production on a homogeneous base. A sensitivity analysis involving 225 well geometry and geothermal source conditions has been performed to analyze the exergy efficiency of considered user systems in different contexts.

The results show a good potential of district heating application as it ensures high values of both useful thermal power and exergy efficiency. Additionally, this application results one of the most robust user strategies as it ensures good performances at many WBHX depths and source temperature. The Absorption chiller alone does not result in good performances as this technology has a too low exergy efficiency in producing cooling energy. Power production through ORC technology shows performances similar to the typical values of geothermal binary plants. However, it can be employed in a limited number of cases, namely when the geothermal source has a sufficient temperature. Moreover, the final performance is affected by a notable uncertainty as the results show a great sensibility to the ground source conditions, which are generally hard to be assessed in practical cases. The employment of the cascade solution as the ORC+DH configuration is confirmed to be attractive in terms of both energy and exergy efficiency, however, the above-mentioned drawbacks on power production remains. Future developments of the present work involve the analysis of other end-user applications and system layouts. Additionally, quantitative criteria to select the most suitable application strategy will be investigated.

Conflicts of Interest: The authors declare no conflict of interest.

Nomenclature

c	specific heat capacity	[J/kg K]
$\dot{e}x$	specific exergy	[kJ/kg]
$\dot{E}_x$	exergy rate	[W]
K_g	temperature gradient	[°C/100 m]
$\dot{I}$	exergy destruction	[W]
IQR	interquartile range	
k	convective heat transfer	[W/m² K]
H	total length of the well	[m]
$\dot{m}$	mass flow rate	[kg/s]
p	pressure	[bar, MPa]
$\dot{Q}$	total thermal power	[W]
R	thermal resistance	[mK/W]
r	radius	[mm]
T	temperature	[K or °C]
t	time	[s]
$\dot{W}$	mechanical/electrical power	[W]
z	depth	[m]

Greek symbols

α	thermal diffusivity	[m²/s]
η	efficiency	
λ	thermal conductivity	[W/m K]
ϱ	density	[kg/m³]

Subscripts, superscripts, acronyms

a	ambient state
ABSC	absorption chiller
CP	circulation pump
CT	cooling tower
DH	district heating
DSH+COND	desuperheater + condenser
dw	downward
EER	energy efficiency ratio
EVA	evaporator
f	fluid
gen	generator
HEx	heat-exchanger
II	second-law
i	inner
in	inlet
o	outer
ORC	organic ranking cycle
out	outlet
P	pump
PH	preheater
ret	return
s	soil property
sup	supply

SH	superheater
T	turbine
up	upward
w	water
WBHX	WellBore Heat eXchanger
0	reference state

References

1. IRENA. *Renewable Capacity Statistics 2019*; International Renewable Energy Agency (IRENA): Abu Dhabi, UAE, 2019; ISBN 978-92-9260-123-2.
2. Kujawa, T.; Nowak, W.; Stachel, A.A. Utilization of existing deep geological wells for acquisitions of geothermal energy. *Energy* **2006**, *31*, 650–664.
3. Wang, Z.; McClure, M.W.; Horne, R.N. A single-well EGS configuration using a thermosiphon. In Proceedings of the Thirty-Fourth Workshop on Geothermal Reservoir Engineering Stanford University, Stanford, CA, USA, 9–11 February 2009.
4. Taleghani, A.D. An improved closed-loop heat extraction method for geothermal resources. *J. Energy Resour. Technol. ASME* **2013**, *135*, doi: 10.1115/1.4023175.
5. Akhmadullin, I.; Tyagi, M. Design and analysis of electric power production unit for low enthalpy geothermal reservoir applications. *Int. J. Environ. Chem. Ecol. Geol. Geophys. Eng.* **2014**, *1*, 6.
6. Mokhtari, H.; Hadiannasab, H.; Mostafavi, M.; Ahmadibeni, A. Determination of optimum geothermal Rankine cycle parameters utilizing coaxial heat exchanger. *Energy* **2016**, *102*, 260–275.
7. Renaud, T.; Verdin, P.; Falcone, G. Numerical simulation of a Deep Borehole Heat Exchanger in the Krafla geothermal system. *Int. J. Heat Mass Transf.* **2019**, *143*, 118496.
8. Nalla, G.; Shook, G.M.; Mines, G.L.; Bloomfield, K.K. Parametric sensitivity study of operating and design variables in wellbore heat exchangers. *Geothermics* **2005**, *34*, 330–346.
9. Morita, K.; Bollmeier, W.S.; Mizogami, H. An experiment to prove the concept of the downhole coaxial heat exchanger (DCHE) in Hawaii. *Trans. Geotherm. Res. Council* **1992**, *16*, 9–16.
10. Kohl, T.; Brenni, R.; Eugster, W. System performance of a deep borehole heat exchanger. *Geothermics* **2002**, *31*, 687–708.
11. Wang, Z.; Wang, F.; Liu, J.; Ma, Z.; Han, E.; Song, M. Field test and numerical investigation on the heat transfer characteristics and optimal design of the heat exchangers of a deep borehole ground source heat pump system. *Energy Convers. Manag.* **2017**, *153*, 603–615.
12. Dai, C.; Shi, Y.; Zeng, L.; Li, J.; Lei, H. Heat Extraction Performance of a Deep Downhole Heat Exchanger. *Energy Procedia* **2019**, *158*, 5602–5607.
13. Galoppi, G.; Biliotti, D.; Ferrara, G.; Carnevale, E.A.; Ferrari, L. Feasibility study of a geothermal power plant with a double-pipe heat exchanger. *Energy Procedia* **2015**, *81*, 193–204.
14. Alimonti, C.; Soldo, E.; Berardi, D.; Bocchetti, D. A comparison between energy conversion systems for a power plant in Campi Flegrei geothermal district based on a WellBore Heat eXchanger. In Proceedings of the European Geothermal Congress 2016, Strasbourg, France, 19–23 September 2016.
15. Alimonti, C.; Soldo, E. Study of geothermal power generation from a very deep oil well with a wellbore heat exchanger. *Renew. Energy* **2016**, *86*, 292–301.
16. Davis, A.P.; Michaelides, E.E. Geothermal power production from abandoned oil wells. *Energy* **2009**, *34*, 866–872.
17. Templeton, J.D.; Ghoreishi-Madiseh, S.A.; Hassani, F.; Al-Khawaja, M.J. Abandoned petroleum wells as sustainable sources of geothermal. *Energy* **2014**, *70*, 366–373.
18. Feng, Y.; Tyagi, M.; White, C.D. A downhole heat exchanger for horizontal wells in low-enthalpy geopressured geothermal brine reservoirs. *Geothermics* **2015**, *53*, 368–378.
19. Noorollahi, Y.; Pourarshad, M.; Jalilinasrabady, S.; Yousefi, H. Numerical simulation of power production from abandoned oil wells in Ahwaz oil field in southern Iran. *Geothermics* **2015**, *55*, 16–23.
20. Wight, N.M.; Bennett, N.S. Geothermal energy from abandoned oil and gas wells using water in combination with a closed wellbore. *Appl. Therm. Energy* **2015**, *89*, 908–915.
21. Mottaghy, D.; Dijkshoorn, L. Implementing an effective finite difference formulation for borehole heat exchangers into a heat and mass transport code. *Renew. Energy* **2012**, *45*, 59–71.

22. Macenić, M.; Kurevija, T. Revitalization of abandoned oil and gas wells for a geothermal heat exploitation by means of closed circulation: Case study of the deep dry well Pčelić-1. *Interpretation* **2018**, *6*, 1–9.
23. DiPippo, R. Second law assessment of binary generating power from low-temperature geothermal fluids. *Geothermics* **2004**, *33*, 565–586.
24. Kotas, T.J. *The Exergy Method of Thermal Plant Analysis*; Krieger Publishing Company: Malabar, FL, USA, 1995.
25. Lee, K.C. Classification of geothermal resources by exergy. *Geothermics* **2001**, *30*, 431–442.
26. Barbacki, A. Classification of geothermal resources in Poland by exergy analysis—Comparative study. Renewable and Sustainable. *Energy Rev.* **2012**, *16*, 123–128.
27. Ramajo, H.; Tritlla, J.; Levresse, G.; Tello-Hinojosa, E.; Ramírez, G.; Pérez, H. New SExI tools to evaluate the evolution and anthropic disturbance ingeothermal fields: The case of Los Azufres geothermal field, México. *Rev. Mex. Cienc. Geol.* **2010**, *27*, 520–529.
28. Yari, M. Exergetic analysis of various types of geothermal power plants. *Renew. Energy* **2010**, *35*, 112–121.
29. Ganjehsarabi, H.; Gungor, A.; Dincer, I. Exergetic performance analysis of Dora II geothermal power plant in Turkey. *Energy* **2012**, *46*, 101–108.
30. Fallah, M.; Akbarpour Ghiasi, R.; Hasani Mokarram, N. A comprehensive comparison among different types of geothermal plants from exergy and thermoeconomic points of view. *Therm. Sci. Eng. Prog.* **2018**, *5*, 15–24.
31. Ozgener, L.; Hepbasli, A.; Dincer, I. Thermo-mechanical exergy analysis of Balcova geothermal district heating system in Izmir, Turkey. *ASME J. Energy Resour. Technol.* **2004**, *126*, 293–301.
32. Ozgener, L.; Hepbasli, A.; Dincer, I. Energy and exergy analysis of Salihli geothermal district heating system in Manisa, Turkey. *Int. J. Energy Res.* **2005**, *29*, 393–408.
33. Ozgener, L.; Hepbasli, A.; Dincer, I. Energy and exergy analysis of the Gonen geothermal district heating system, Turkey. *Geothermics* **2005**, *34*, 632–645.
34. Hepbasli, A. Thermodynamic analysis of a ground-source heat pump system for district heating. *Int. J. Energy Res.* **2005**, *29*, 671–687.
35. Kang, S.; Li, H.; Liu, L.; Lei, J.; Zhang, G. Exergy analysis of a novel CHP–GSHP coupling system. *Appl. Therm. Eng.* **2016**, *93*, 308–314.
36. Alimonti, C.; Conti, P.; Soldo, E. A comprehensive exergy evaluation of a deep borehole heat exchanger coupled with a ORC plant: The case study of Campi Flegrei. *Energy* **2019**, *189*, 116100.
37. Casarosa, C.; Conti, P.; Franco, A.; Grassi, W.; Testi, D. Analysis of thermodynamic losses in ground source heat pumps and their influence on overall system performance. *J. Phys. Conf. Ser.* **2014**, *547*, 012006.
38. NIST. *Standard Reference Database 23: Reference Fluid Thermodynamic and Transport Properties-REFPROP*; Version 9.1; National Institute of Standards and Technology, Standard Reference Data Program: Gaithersburg, Maryland, 2013.
39. Conti P, Testi D, Grassi W: Revised heat transfer modeling of double-U vertical ground-coupled heat exchangers. *Appl. Therm. Eng.* **2016**, *106*, 1257–1267.
40. Conti P: Dimensionless maps for the validity of analytical ground heat transfer models for GSHP applications. *Energies* **2016**, *9*, 890.